

# Structural Insights into the Interaction of Platinum-based Inhibitors with the Alzheimer's Disease Amyloid- $\beta$ Peptide

Victor A. Streltsov\*, V. Chandana Epa, Simon James, Quentin Churches, Joanne M. Caine, Vijaya B. Kenche, Kevin J. Barnham

## Electronic Supporting Information

### Experimental Section

**Pt complexes.** Cisplatin and Pt<sup>II</sup>-1,10-phenanthroline were purchased from Aldrich. Stock solutions of Pt-compounds were prepared by dissolving known amounts of the compounds in dimethyl sulfoxide (DMSO) to give a final concentration of 20 mM. Stock solutions in DMSO were made just before complexing with A $\beta$  to avoid formation of adducted compounds with different therapeutic and biological characteristics.<sup>1</sup>

**A $\beta$  Peptide Preparation.** Synthetic A $\beta$ <sub>16</sub> or A $\beta$ <sub>42</sub> peptide (W.M. Keck Facility, Yale University) was dissolved from a lyophilized powder in TFA and dried under a nitrogen stream. The remaining film was dissolved in 100% 1,1,1,3,3,3-hexafluoro-2-propanol (HFIP) to a concentration of 1 mg/mL, sonicated 5 min in a water bath and dried under a nitrogen stream. The HFIP treatment was repeated twice more but on the final dissolving, the peptide was aliquoted into microcentrifuge tubes, put under a nitrogen stream till dry and finally dried under vacuum for 1 h. The aliquots were then stored at -20 °C. Immediately prior to use, the HFIP-treated A $\beta$ <sub>42</sub> was dissolved in DMSO and the concentration determined by absorbance at 280nm on a diluted sample (1 to 35 water) using an extinction coefficient of 1490 M<sup>-1</sup>cm<sup>-1</sup>.

**Complexing.** For X-ray absorption, DLS and MS data collection, aliquots of A $\beta$ <sub>16</sub> and A $\beta$ <sub>42</sub> peptides were dissolved in phosphate buffer, PB, (pH 7.5) and in DMSO and PB, respectively, then complexed with cisplatin or Pt<sup>II</sup>-1,10-phenanthroline at a 1:1 molar ratio with the final concentration of 2 mM. Complexes were incubated for about 1 h at room temperature before experiments. Finally, glycerol (~20%) was added to the sample solution as a cryoprotectant before x-ray absorption data collection.

**Dynamic Light Scattering.** For dynamic light scattering (DLS) experiments the A $\beta$ <sub>42</sub> in DMSO was diluted into 50 mM Tris pH 8 to a final concentration of 100  $\mu$ M. Compounds were added in 1:5 molar ratio of A $\beta$ <sub>42</sub>:Pt-compound. (Due to the limit of solubility of the Pt compounds, the experiments cannot be done at 1:1 ratio.) Solvent and compound alone controls were made up at the concentrations used in the A $\beta$ <sub>42</sub>:Pt experiments. All reaction mixtures were filtered through 0.2 nm syringe filter before loading, in quadruplicate, 20  $\mu$ L into a Greiner 384-well low volume glass bottom plate. A total time of 20 min elapsed between the addition of the A $\beta$ <sub>42</sub> to the compound and the acquiring of data from the plate. DLS was completed using Dyna Pro Nano Star plate reader at the Collaborative Crystallisation Centre (CSIRO) at laser wavelength 830 nm, with temperature control capacity and auto-attenuation function. The measurements were taken at 25°C, which ensures a large enough delta between measurement temperature and room temperature to ensure stability. To ensure accurate readings, the final distribution was taken from an accumulation of 50 individual 5 second DLS collections. Hydrodynamic radius,  $R_h$ , was calculated from translation diffusion coefficient by the Stokes–Einstein relationship.

The DLS results (Figure 1S) show that A $\beta$ <sub>42</sub> alone forms a polydisperse, approximately bimodal solution with an average hydrodynamic radius of the first peak of ~6 nm. The radius for A $\beta$ <sub>42</sub> monomer has been reported in the literature between 0.9-1.6 nm,<sup>2,3</sup> so the size of the A $\beta$ <sub>42</sub> in our solution would suggest that it was already aggregating by the time it was submitted to DLS at t=0-20 min. The additions at t=0 of **4** still yielded a polydispersed solution at t=20 min with two intensity peaks at hydrodynamic radii ( $R_h$ ) of ~6 nm and ~138 nm which correspond to small and larger aggregates, correspondently. This distribution did not change after 2 h of incubation while the control A $\beta$ <sub>42</sub> continued aggregating. Reduction of the DLS intensity for A $\beta$ <sub>42</sub> control (non-complexed) species with  $R_h$ ~70-100 nm after 2 h and their complete disappearance of after 12 h suggested their conversion to significantly bigger aggregates (fibrils) with  $R_h$ >1000 nm (Figure 1S). DLS experiments on the Pt-compounds alone yielded poor data.

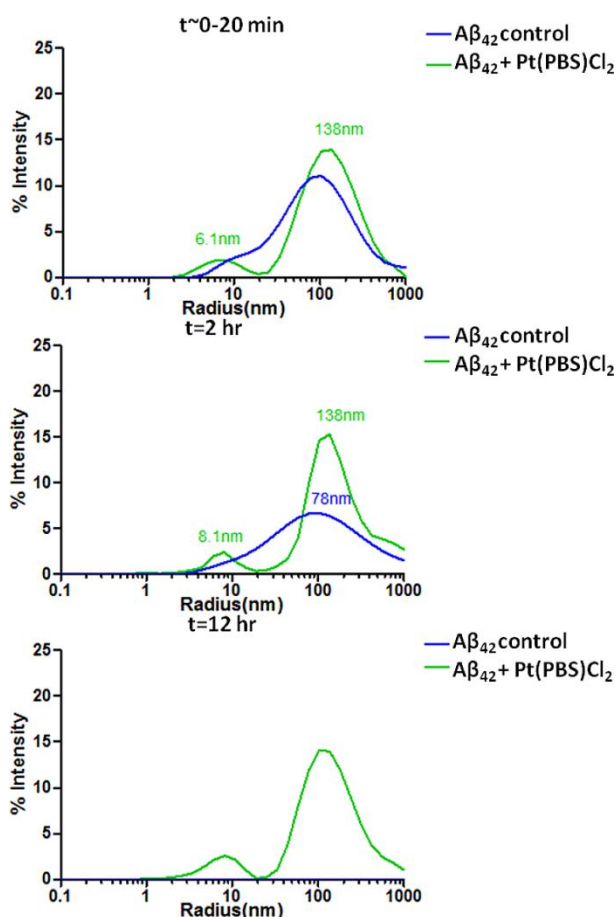


**Figure 1S.** DLS profiles for  $A\beta_{42}$  (controls) and complexed with  $Pt(PBS)Cl_2$  (**4**) at  $t \sim 0, 2$  and  $12$  h.

**MALDI-TOF Mass Spectrometry.** The dried  $A\beta_{16}$  or  $A\beta_{42}$  film was re-dissolved and prepared for incubation with Pt-compounds prior to analysis with MALDI-TOF as described previously.<sup>4</sup> Briefly,  $A\beta_{16}$  or  $A\beta_{42}$  was dissolved in 222  $\mu$ l of a freshly prepared mixture consisting of  $CH_3CN / 300 \mu M Na_2CO_3 / 250 mM NaOH$  (48.3:48.3:3.4 % v/v/v) by brief sonication and vortexing. The resulting alkaline  $A\beta_{16}$  or  $A\beta_{42}$  solution ( $\sim 500 \mu M$ ) was diluted 1:10 with PB (10 mM, pH 7.2) containing NaCl (11 mM) to obtain a 50  $\mu M$   $A\beta_{42}$  solution at final pH 7.6 and an NaCl concentration of 10 mM. Where appropriate either cisplatin (cisPt),  $Pt(1,10\text{-phenanthroline})Cl_2$  or  $Pt(4,7\text{-dipheyl-[1,10]phenanthroline}disulphonate)Cl_2$  ( $Pt(PBS)Cl_2$ ) was added to the reaction mixture from a stock solution of PB buffer containing 1 % (v/v) DMSO. Therefore, final assay conditions were as follows:  $\sim 50 \mu M$   $A\beta_{42}$  in phosphate buffer (8.7 mM) containing 10 mM NaCl, 14.5  $\mu M$   $Na_2CO_3$ , 0.85 mM NaOH, 8.2 % acetonitrile and 4-5  $\mu M$  of Pt compound where indicated (final pH 7.6). The  $A\beta_{16}$  or  $A\beta_{42}$  solutions were briefly sonicated and incubated at 37 °C by a Thermomixer Comfort (Eppendorf South Pacific, North Ryde Australia) with gentle agitation. Aliquots were then taken for MALDI-TOF analysis at two time points ( $t = 0$  and  $t = 2$  h).  $A\beta_{16}$  or  $A\beta_{42}$  MALDI-TOF MS analyses were performed using a Ultraflex extreme (Bruker) equipped with a pulsed nitrogen laser (337 nm) operating at 1000 Hz. Ternary complex positive ion spectra were acquired in linear mode over an  $m/z$  range from 650 to 9000 Da using a 2 kV accelerating voltage, a 25 kV grid voltage, and a pulsed ion extraction time of 120 ns. The spectrum for each spot was obtained by averaging the results of 1500 laser shots. The analysis was performed by spotting on the target plate 1.0  $\mu$ L of the sample mixed with an equal volume of the matrix solution, 30 mg/ml sinapinic acid (Sigma-Aldrich), in  $CH_3CN/H_2O$  (50:50 % v/v) containing 0.1 % (v/v) trifluoroacetic acid (Sigma-Aldrich).

**X-ray absorption data collection.** The solutions of cisPt or  $Pt(PBS)Cl_2$  in DMSO and solution samples of complexes with  $A\beta_{16}$  or  $A\beta_{42}$  peptides were injected into 100 mL Teflon (DuPont, Wilmington, Delaware) cells made with two Kapton (Goodfellow Cambridge, Cambridge, UK) windows and rapidly frozen in liquid nitrogen. For each sample a series of four Pt L<sub>III</sub> edge ( $E_0 = 11564$  eV) x-ray absorption spectrum scans up to  $k = 12 \text{ \AA}^{-1}$  were obtained in a fluorescence mode at low  $T \approx 15$  K using a helium displax cryostat and a 100-element liquid  $N_2$ -cooled Ge detector. Each scan was collected at different sample spot to monitor radiation damage. Radiation damage of samples was also tested by quick XANES measurement in the 30 min exposure intervals (Figure 2S). The incident x-ray intensity was monitored using an ionization chamber. The stability of the monochromator energy was checked for all spectra by the simultaneous accumulation of a Pt foil spectrum by transmittance. The experiments were conducted at the Australian synchrotron XAS beamline (1.9 T Wiggler).

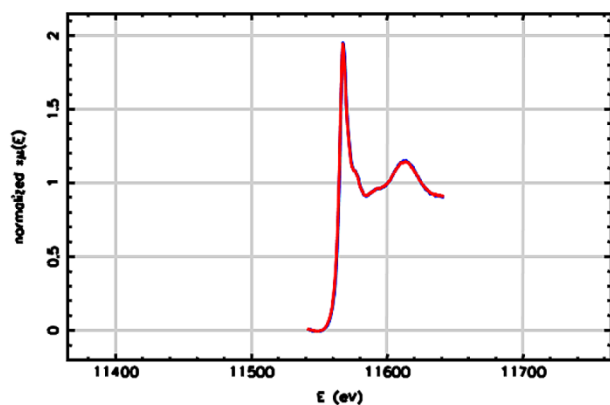


**Figure 2S.** Example of XANES scans before and after long exposure (30min) for  $A\beta_{42}$ -Pt(BPS)Cl<sub>2</sub> complex.

**Quantum Mechanical Calculations.** These were done in gas phase using the MPW1PW91 density functional<sup>5</sup> and the SDD basis set<sup>6,7</sup> with the Gaussian 03 suite of programs. The appropriateness of this level of theory, the density functional, and the basis set was confirmed by computing the optimized geometries for two high-resolution crystal structures from the Cambridge Structural Database (<http://www.ccdc.cam.ac.uk/products/csd/>), viz. that of cis-Dichloro-ammine-(dimethylsulfoxide) platinum(II)<sup>8</sup> (CSD ID: CASXPT) and of (benzo)(h)quinolin-10-yl)-chloro-(dimethyl sulfoxide-S)-platinum(II)<sup>9</sup> (CSD ID: JISPEH). All geometry optimizations were performed with the modified GDIIS<sup>10</sup> algorithm and tight convergence criteria. Stationary points were checked for true energy minima by carrying out frequency calculations. The computed geometries of CASXPT and JISPEH show (see Table S1 in the Supplementary Information) that the Pt bond distances and Pt bond angles agree with the experimental (crystal) values to 0.14 Å or better and 3.60 or better, respectively. Firstly, the structures of cisPt and Pt(PBS)Cl<sub>2</sub> were modeled. In the latter, the sulphonate groups were modeled at the para-positions in the phenyl moieties. The phenyl rings and sulphonate groups attached to the phenanthroline moiety are sufficiently distant from the Pt centre that they affect the EXAFS spectra only minimally. For all the modeling, Pt was considered to be in an oxidation state of +2 and have an approximately planar, tetra-coordinated first coordination shell.

**Table 1S.** Geometry parameters for the crystal structures compared to the DFT computed values (bond lengths in Å, bond angles in degrees)

Compound CSD ID	Bond or Angle	Experimental (crystal)	Calculated (DFT)
<b>JISPEH</b>	Pt-N	2.06	2.03
	Pt-C	2.01	2.01
	Pt-Cl	2.40	2.49
	Pt-S	2.21	2.35
	N-Pt-Cl	91.07	94.27
	S-Pt-Cl	89.24	85.67
<b>CASXPT</b>	Pt-N	2.03	2.07
	Pt-Cl	2.30-2.32	2.34-2.38
	Pt-S	2.19	2.33
	N-Pt-Cl1	87.85	87.24
	S-Pt-Cl2	89.65	88.51
	Cl1-Pt-Cl2	92.16	95.46

In modeling cisplatin and Pt(PBS)Cl<sub>2</sub> bound to A $\beta$ , the following model structures were constructed and their geometries optimized (Table 2S). In all cases, the central Pt was taken to have an approximately planar, tetra-coordinated geometry. These were considered the only plausible initial structures.

1. cisPt bound to A $\beta_{16}$ : Pt coordinated to 2xNH<sub>3</sub>, 1xCl, 1ximidazole; 2xNH<sub>3</sub>, 2ximidazole; and 1xmethyl amine, 3ximidazole. Here, the Pt-N(imidazole), Pt-N(NH<sub>3</sub>), and Pt-Cl bond lengths were 2.0, 2.1, and 2.35 Å, respectively.
2. cisPt bound to A $\beta_{42}$  (i.e. methionine ligand): Pt coordinated to 1xmethyl ethyl thioether, 3ximidazole; and 1xNH<sub>3</sub>, 1xmethyl ethyl thioether, 2ximidazole. Here, the Pt-S bond length in the optimized model systems was 2.4 Å.
3. Pt(BPS)Cl<sub>2</sub> bound to A $\beta$ : Pt coordinated to 1xCl, 1ximidazole, 1xphenanthroline; and 2ximidazole, 1xphenanthroline. Here all the Pt-N bond lengths were 2.0 Å while the Pt-Cl bond length was 2.36 Å.

**Table 2S.** Geometries of the final optimized complex structures in xyz format

<b>Pt(NH<sub>3</sub>)<sub>2</sub>Cl-His</b>	<b>Pt(NH<sub>3</sub>)<sub>2</sub>-His<sub>2</sub></b>	<b>Pt(NH<sub>3</sub>)-His<sub>3</sub></b>	<b>Pt(NH<sub>3</sub>)-His<sub>2</sub>Met</b>
x y z	x y z	x y z	x y z
Pt -0.1030 0.2450 0.0860	Pt -0.6270 -0.1100 0.0530	Pt 0.0060 -0.3440 -0.0860	Pt 0.0000 0.0000 0.0000
Cl 1.4600 -1.4350 0.6090	N -2.7190 -0.1260 0.0420	N 2.0350 -0.2830 -0.0570	N 0.3790 -2.0320 -0.2810
N 1.5380 1.5240 0.1280	N -0.5270 -2.1690 0.4100	C 2.8150 -0.0300 1.0080	N -0.4560 1.9620 0.1890
N -1.5050 1.7520 -0.3250	N 1.3940 -0.0710 0.0310	C 2.8790 -0.4990 -1.1530	C -1.0080 2.5720 1.2520
N -1.5760 -1.1280 0.0640	C 2.2060 0.3730 1.0080	C 4.1820 -0.3760 -0.7280	C -0.2900 2.9250 -0.8130
C -1.8090 -2.0150 1.0430	C 2.2040 -0.4820 -1.0360	N 4.1170 -0.0830 0.6260	C -0.7510 4.1290 -0.3330
C -2.4340 -1.4340 -0.9960	C 3.5180 -0.2800 -0.6810	N -0.0820 1.6730 0.0930	N -1.1950 3.8830 0.9590
C -3.1980 -2.5190 -0.6350	N 3.4930 0.2540 0.5990	C 0.5650 2.5770 -0.6630	N -1.9620 -0.4770 0.2200
N -2.7910 -2.8640 0.6460	N -0.6950 1.8850 -0.2630	C -0.8470 2.3780 1.0270	C -2.9430 -0.2740 -0.6770
	C -0.4620 2.5290 -1.4210	C -0.6480 3.7230 0.8230	C -2.5400 -1.0650 1.3530
	C -0.9690 2.8540 0.7110	N 0.2380 3.8240 -0.2400	C -3.8880 -1.2150 1.1190
	C -0.9000 4.0930 0.1170	N -2.0220 -0.4360 -0.1310	N -4.1150 -0.7130 -0.1540
	N -0.5820 3.8640 -1.2140	C -2.8140 -0.1370 -1.1760	S 2.2840 0.6710 -0.3540
		C -2.8540 -0.7960 0.9350	C 2.7630 1.8180 1.0480
		C -4.1610 -0.7120 0.5130	C 3.5110 -0.7610 -0.1010
		N -4.1100 -0.2990 -0.8100	C 3.5940 -1.3130 1.3150
		N 0.0810 -2.4210 -0.2620	
		C 0.3900 -3.1620 1.0120	
<b>Pt-His<sub>3</sub>Met</b>	<b>Pt(BPS)Cl-His</b>	<b>Pt(BPS)-His<sub>2</sub></b>	
x y z	x y z	x y z	
Pt 0.0000 0.0000 -0.0000	Pt 0.0000 0.0000 -0.0000	Pt 0.0000 0.0000 -0.0000	
N 2.0010 0.3360 -0.0040	N 1.8250 0.8650 0.0270	N 1.3300 -1.5190 0.2220	
C 2.8460 0.2930 1.0400	C 2.8060 0.6270 -0.8530	C 1.8960 -2.2460 -0.7560	
C 2.7370 0.7350 -1.1230	C 2.3550 1.6560 1.0490	C 1.7800 -2.0310 1.4430	
C 4.0440 0.9280 -0.7370	C 3.6780 1.9030 0.7630	C 2.6330 -3.0790 1.1840	
N 4.0890 0.6450 0.6200	N 3.9380 1.2490 -0.4350	N 2.6900 -3.1950 -0.1980	
N -0.2950 1.9880 0.2880	C -2.1690 -2.1320 0.0700	N -1.4500 -1.3890 -0.3040	
C -0.8250 2.8460 -0.5990	C -2.8600 0.1080 0.0380	C -2.0770 -2.1200 0.6330	
C 0.0210 2.7140 1.4390	C -3.5160 -2.5560 0.1120	C -1.9390 -1.7930 -1.5500	
C -0.3300 4.0280 1.2320	C -4.5440 -1.6220 0.1160	C -2.8760 -2.7800 -1.3480	
N -0.8550 4.0860 -0.0510	C -0.6760 2.9830 -0.1300	N -2.9460 -2.9670 0.0260	
S 0.2020 -2.3490 -0.4410	C -2.4580 1.4710 -0.0110	C 2.6950 1.3710 0.4790	
C 1.9830 -2.8490 -0.6980	C -1.5770 4.0670 -0.1600	C 0.8160 2.7410 0.1940	
C -0.2530 -3.2720 1.1580	C -2.9470 3.8360 -0.1070	C 3.5170 2.5060 0.6390	
C 0.5470 -2.8580 2.3820	N -1.1030 1.7130 -0.0490	C 2.9650 3.7790 0.5740	
N -2.0110 -0.2820 -0.0240	N -1.8540 -0.8280 0.0340	C -2.5720 1.6140 -0.3960	
C -2.7380 -0.8330 -1.0130	C -3.4220 2.5020 -0.0330	C -0.5860 2.8050 -0.0400	
C -2.8970 0.0950 0.9900	C -4.2260 -0.2390 0.0760	C -3.2970 2.8200 -0.4910	
C -4.1710 -0.2420 0.5980	C -4.8140 2.1370 0.0120	C -2.6410 4.0380 -0.3560	
N -4.0470 -0.8190 -0.6580	C -5.2000 0.8220 0.0660	N -1.2460 1.6050 -0.1770	
	Cl 1.1210 -2.0750 -0.0010	N 1.3740 1.4840 0.2620	
		C -1.2420 4.0520 -0.1220	
		C 1.5720 3.9230 0.3440	
		C -0.4600 5.2510 0.0330	
		C 0.8930 5.1890 0.2570	

*X-ray absorption data processing.* The EXAFS (Extended X-ray Absorption Fine Structure) oscillations  $\chi(k)$  were extracted from the experimentally measured absorption coefficient using an automated background subtraction AUTOBK algorithm implemented in the program ATHENA<sup>11</sup>. The EXAFS oscillations  $\chi(k)$  were quantitatively analyzed by the ARTEMIS<sup>11</sup> program, also an interface to IFEFFIT<sup>12</sup>, using *ab initio* theoretical amplitude, phase, and mean-free path factors calculated by FEFF8.4<sup>13</sup>. Constrained and restrained refinement procedures were used to minimize the number of free parameters in the least-squares refinement to increase the degree of determinacy of the model. The fitting procedure consisted of successive cycles of restrained simultaneous refinements with  $k^1$ ,  $k^2$ , and  $k^3$  weights of  $\chi(k)$  data in  $k$ -space with  $2.5 \leq k \leq 12.5 \text{ \AA}^{-1}$  and  $3 \leq k \leq 11 \text{ \AA}^{-1}$  for  $\text{A}\beta$  complexes with cisPt and Pt(BPS)Cl<sub>2</sub>, respectively, and followed by refinement with  $k^3$  in R-space,  $0 \leq R \leq 5.0 \text{ \AA}$ , for all complexes. All multiple scattering (MS) contributions >10% and  $l=4$  (triple scattering paths with four legs) were included in the refined model. For imidazole's three refinable parameters are considered: the Pt-N distance ( $r$ ), the in-plane rotation angle ( $\varphi$ ), and the out-of-plane tilt angle ( $\theta$ ). Further details and initial structural parameters for histidines were similar to those in our EXAFS analysis of  $\text{A}\beta_{16}\text{Cu}$  complex.<sup>14</sup> The similarity in the XANES and EXAFS regions between the  $\text{A}\beta_{16}\text{-Pt(PBS)Cl}_2$  and  $\text{A}\beta_{42}\text{-Pt(PBS)Cl}_2$  groups of measurements suggested that geometry of the Pt<sup>2+</sup> coordination does not change significantly across the samples. Therefore we have attempted a multiple EXAFS data refinement in these two sets of measurements. Each of the two DFT optimized global models was used to simultaneously fit the experimental information extracted from the EXAFS regions of  $\text{A}\beta_{16}\text{-Pt(PBS)Cl}_2$  and  $\text{A}\beta_{42}\text{-Pt(PBS)Cl}_2$  spectra. All structural parameters and  $S_0^2$  remained the same throughout each data and

$\Delta E_0$  was refined for each data set separately. The data sets were weighted by the measurement uncertainties,  $\varepsilon_k$ , in  $k$ -space. The values of  $R$ -factor and  $\chi^2$  (reduced goodness-of-fit) are calculated in  $r$ -space as follows

$$R = \frac{\sum_i^N f(r_i)^2}{\sum_i^N \chi_{data}(r_i)^2}$$

and

$$\chi^2 = \frac{N_{ind}}{\varepsilon_k^2 N(N_{ind} - N_{var})} \sum_{i=1}^N f(r_i)^2, \text{ where the magnitude of the residual } f(r)^2 = f_{xafs}(r)^2 + \sum (w\Delta_{restraint}/\sigma_{restraint})^2 \text{ with } f_{xafs}(r) \text{ defined}$$

as  $f_{xafs}(r) = \chi_{data}(r) - \chi_{model}(r)$ , where  $f(r)$  is the minimized function which consists of the real and imaginary parts of the difference between data  $\chi_{data}(r)$  and model  $\chi_{model}(r)$  XAFS over the fit range  $r$ . The residual (penalty) function  $\Delta_{restraint}$  evaluates 0 if the restraint expression is satisfied or is the difference between the two sides of the restraint expression;  $\sigma_{restraint}$  is the uncertainty value given for the restraint and derived here from the standard deviation of crystallographic structural parameters, and the weight  $w$  (the amplifier) determines the magnitude of the penalty. Final step of refinement was conducted with  $w=1000$ . Further,  $N_{var}$  is the number of variables in the fit;  $N=2(\Delta r)/\delta r$  is the number of data points in  $r$ -space with the grid spacing  $\delta r$ , and  $N_{ind} = \frac{2(\Delta k + \Delta r)}{\pi}$  is the number of independent data points<sup>12, 15</sup> with data ranges  $\Delta r = r_{max} - r_{min}$  and  $\Delta k = k_{max} - k_{min}$  in  $r$ - and  $k$ -space, respectively.

**Table 3S:** Best-fit EXAFS ( $E_0$  in eV) is the photoelectron energy threshold;  $r$  and  $\phi$  refer to the distances (in Å) and the polar angle (in degrees);  $\sigma^2$  - Debye-Waller terms (in Å<sup>2</sup>);  $S_0^2 \approx 1$  - the amplitude reduction factor (core-hole factor);  $n_{ind}$  - the number of independent data points,  $n_{var}$  - the number of refined parameters,  $\chi^2$  and  $R$ -factor are defined in Supporting Information above; estimated standard deviation from least squares is given in parenthesis.)

	A $\beta_{16}$ -cisPt	A $\beta_{42}$ -cisPt	A $\beta_{16}$ /A $\beta_{42}$ -Pt(BPS)Cl <sub>2</sub> <sup>[a]</sup>
$r$ -NH <sub>3</sub> (av) <sup>[b]</sup>	<b>2.03(1)</b>	<b>2.07(2)</b>	
$S_0^2 \times Occ$ <sup>[c]</sup>	0.7(1)	0.2(1)	
$r$ -N(His) (av)	<b>2.04(1)</b>	<b>2.06(2)</b>	<b>1.99(1)</b>
$\phi$ (av) <sup>[d]</sup>	2(2)	5(2)	11(1)
$S_0^2 \times Occ$	0.5(1)	1.4(5)	1.40(9)/1.00(7)
$r$ -N(phen) <sup>[e]</sup> (av)			<b>1.993(5)</b>
$S_0^2 \times Occ$			2.00(7)
$\sigma^2(N)$ <sup>[f]</sup>	0.00158(2)	0.0026(2)	0.0027(4)
$r$ -Cl	<b>2.242(6)</b>		<b>2.228(8)</b>
$S_0^2 \times Occ$	0.82(6)		0.60(9)/1.00(7)
$\sigma^2(Cl)$	0.0022(7)		0.0031(8)
$r$ -S(Met35)		<b>2.306(5)</b>	
$S_0^2 \times Occ$		1.08(8)	
$\sigma^2(S)$		0.0016(4)	0.0031(8)
$\Delta E_0$	0.1(8)	2.3(6)	2.7(8)/3.0(9)
$n_{ind}/n_{var}$	31/13	31/19	50/14
$\varepsilon_k$ <sup>[g]</sup>	0.001	0.0009	0.0015/0.0020
$R$	0.027	0.016	0.022
$\chi^2$	1.51	1.29	1.19

[a] Model simultaneously fitted to two data sets for A $\beta_{16}$  and A $\beta_{42}$  complexed with Pt(BPS)Cl<sub>2</sub>; [b] (av) - averaged values; [c] The occupancy parameter  $Occ$  for each model times the amplitude reduction factor (core-hole factor),  $S_0^2$ , was refined with  $\sigma^2$  terms fixed. The total populations of N(H<sub>3</sub>), N(His) and Cl were refined by fixing to physically meaningful values of  $\sigma^2$  (Debye-Waller terms) (consistent with the literature values of  $2\sigma^2$  of 0.0028(3)-0.0058(7) from EXAFS analysis of four Pt-based anticancer drugs.<sup>16-18</sup> [d] The imidazole in-plane polar angle,  $\phi$ , was refined with corresponding  $r$  parameter fixed; [e] N atoms from phenanthroline motif; [f] Debye-Waller terms for atoms at the higher shell ( $r > 4.0\text{Å}$ ) were adjusted by the estimated coefficient as follows  $\sigma^2(\text{higher shell}) = 3 \times \sigma^2$  (1st shell); [g] data uncertainty.

## References

1. S. J. Fischer, L. M. Benson, A. Fauq, S. Naylor and A. J. Windebank, *Neurotoxicology*, 2008, **29**, 444-452.
2. S. Nag, B. Sarkar, A. Bandyopadhyay, B. Sahoo, V. K. Sreenivasan, M. Kombrabail, C. Muralidharan and S. Maiti, *J. Biol. Chem.*, 2011, **286**, 13827-13833.
3. C. Talmard, L. Guilloureau, Y. Coppel, H. Mazarguil and P. Faller, *ChemBiochem*, 2007, **8**, 163-165.
4. M. Bartolini, M. Naldi, J. Fiori, F. Valle, F. Biscarini, D. V. Nicolau and V. Andrisano, *Anal. Biochem.*, 2011, **414**, 215-225.

5. C. Adamo and V. Barone, *J. Chem. Phys.*, 1998, **108**, 664-675.
6. D. Andrae, U. Haussermann, M. Dolg, H. Stoll and H. Preuss, *Theor. Chim. Acta*, 1990, **77**, 123-141.
7. D. Andrae, U. Haussermann, M. Dolg, H. Stoll and H. Preuss, *Theor. Chim. Acta*, 1991, **78**, 247-266.
8. R. Melanson and F. D. Rochon, *Acta Cryst. B*, 1978, **34**, 941-943.
9. N. Godbert, T. Pugliese, I. Aiello, A. Bellusci, A. Crispini and M. Ghedini, *Eur. J. Inorg. Chem.*, 2007, 5105-5111.
10. P. Csaszar and P. Pulay, *J. Mol. Struct.*, 1984, **114**, 31-34.
11. B. Ravel and M. Newville, *J. Synch. Rad.*, 2005, **12**, 537-541.
12. M. Newville, *J. Synch. Rad.*, 2001, **8**, 322-324.
13. A. L. Ankudinov, A. I. Nesvizhskii and J. J. Rehr, *Phys. Rev.*, 2003, **B67**, 115120.
14. V. A. Streltsov, S. J. Titmuss, V. C. Epa, K. J. Barnham, C. L. Masters and J. N. Varghese, *Biophys. J.*, 2008, **95**, 3447-3456.
15. E. A. Stern, *Phys. Rev.*, 1993, **B48**, 9825-9827.
16. D. Bouvet, A. Michalowicz, S. Crauste-Manciet, D. Brossard and K. Provost, *Inorg. Chem.*, 2006, **45**, 3393-3398.
17. D. Bouvet, A. Michalowicz, S. Crauste-Manciet, E. Curis, I. Nicolis, L. Olivi, G. Vlaic, D. Brossard and K. Provost, *J. Synch. Rad.*, 2006, **13**, 477-483.
18. K. Provost, D. Bouvet-Muller, S. Crauste-Manciet, J. Moscovici, L. Olivi, G. Vlaic and A. Michalowicz, *Biochimie*, 2009, **91**, 1301-1306.